Sixth International Symposium on Turbulence and Shear Flow Phenomena
Seoul, Korea, 22-24 June 2009

DNS OF PASSIVE SCALAR FIELD WITH MEAN GRADIENT IN FRACTAL-GENERATED TURBULENCE

Hiroki Suzuki
Department of Mechanical Science and Engineering,
Nagoya University
Nagoya 464-8603, Japan
hsuzuki@nagoya-u.jp

Kouji Nagata
Department of Mechanical Science and Engineering,
Nagoya University
Nagoya 464-8603, Japan
nagata@nagoya-u.jp

Yasuhiko Sakai
Department of Mechanical Science and Engineering,
Nagoya University
Nagoya 464-8603, Japan
ysakai@mech.nagoya-u.ac.jp

Toshiyuki Hayase
Institute of Fluid Science,
Tohoku University
Sendai 980-8577, Japan
hayase@ifs.tohoku.ac.jp

Takashi Kubo
Department of Mechanical Science and Engineering,
Nagoya University
Nagoya 464-8603, Japan
t-kubo@nagoya-u.jp

ABSTRACT

Turbulent flow field and passive scalar field in the spatially developing grid-generated turbulence are investigated by means of the direct numerical simulation (DNS). Two types of grids are numerically constructed using a immersed boundary method: the one is a classical biplane square grid and the other is a fractal grid which was firstly used in a wind tunnel by Hurst and Vassilicos (2007) and Seoud and Vassilicos (2007). Two types of passive scalar fields are calculated: the one is a diffusion of a passive scalar with a constant mean gradient and the other is a scalar mixing layer. To ensure the numerical accuracy, fully conservative high order accurate finite different schemes for full staggerd grid system are used. Fundermental flow and scalar fields are presented in this paper.

INTRODUCTION

Grid generated turbulence using a biplane square grid has been widely used to generate nearly isotropic turbulence in both wind tunnel and water channel. Recently, turbulence generated by " fractal grids " has been experimentally investigated by Hurst and Vassilicos (2007) and Seoud and Vassilicos (2007). Hurst and Vassilicos (2007) experimented with total 21 different planar fractal grids and investigated the turbulence characteristics generated by these fractal grids. Seoud and Vassilicos (2007) investigate the case of square type fractal grid in detail. Their experimental results have shown that the fractal grids generate unusually high turbulence intensities compared with " classical " grid turbulence. Moreover, they found that the fractal forcing by the fractal grids modifies turbulence so deeply that dissipation, spectra and evolution of integral and Taylor micro scales exhibit quite unusual behaviors, which are completely different from the classical turbulent theory.

The study on fractal-generated turbulence has just started (Mazzi and Vassilicos, 2004; Hurst and Vassilicos, 2007; Seoud and Vassilicos, 2007; Laizet and Vassilicos, 2008; Laizet et al., 2008; Nagata et al., 2009), and more extensive studies would be required for the full understanding of the fractal-generated turbulence. Especially, turbulent diffusion of a passive scalar in the fractal-generated turbulence has not been well understood.

The purpose of this study is to investigate the flow field

Table 1: Grids parameters and scalar conditions

RunID	grid type	N	D_f	t_r	σ	Re_M	Pr	scalar conditions
bCGT0	biplane square rod grid	1	2.0	1.0	0.36	2500	0.71	uniform scalar gradient
bCGT1	biplane square rod grid	1	2.0	1.0	0.36	2500	0.71	scalar mixing layer
sFGT0	fractal square grid	4	2.0	8.5	0.36	2500	0.71	uniform scalar gradient
sFGT1	fractal square grid	4	2.0	5.0	0.36	2500	0.71	scalar mixing layer
sFGT2	fractal square grid	4	2.0	8.5	0.36	2500	0.71	scalar mixing layer
sFGT3	fractal square grid	4	2.0	13.0	0.36	2500	0.71	scalar mixing layer

and turbulent diffusion of a passive scalar in the spatially developing fractal-generated turbulence by means of the direct numerical simulation (DNS). Two types of passive scalar fields are calculated: the one is a diffusion of a passive scalar with a constant mean gradient and the other is a scalar mixing layer (Nagata and Komori, 2000, 2001). The comparisons of turbulence and scalar diffusion fields between the classical grid turbulence and the fractal generated turbulence at the same mesh Reynolds number are shown in this paper.

FRACTAL GRID

Figure 1 shows the schematic of the fractal square grid. M_i is the length of the bar and d_i is thickness at iteration i, respectively. The grid parameters are listed in Table 1. The reader may refer to Hurst and Vassilicos (2007) for details of the grids. The computation for a classical biplane square grid (Comte-Bellot and Corrsin, 1966) is also performed for comparison. In this study, D_f is chosen as $D_f = 2.0$ (space filling), since the space filling grids have been found to return the best homogeneity (Hurst and Vassilicos, 2007). The solidity σ of the grid is 0.36 to compare the flow field generated by the fractal grids with that by the classical grid at the same blockage ratio. Note that $\sigma = 0.3 \sim 0.4$ is a typical value for a classical grid, and $\sigma = 0.25$ for the fractal square grids investigated in the previous experiments (Hurst and Vassilicos, 2007 ; Seoud and Vassilicos, 2007) would be too small for a classical grid. The thickness ratio $t_r = d_0 / d_N$ of the grid, which is one of the important parameter (Hurst and Vassilicos, 2007), is 5.0, 8.5 and 13.0. In the present DNS, the entire bars have square cross section, although all the bars have the same thickness in the direction of mean flow in the previous experiments (Hurst and Vassilicos, 2007 ; Seoud and Vassilicos, 2007) and DNS (Laizet and Vassilicos, 2008; Laizet et al., 2008). The effective mesh size for the fractal grids (Hurst and Vassilicos, 2007) is defined as

$$M_{eff} = \frac{4T^2}{P_M}\sqrt{1-\sigma}, \tag{1}$$

where T^2 is the cross-sectional area of the channel and P_M is the fractal perimeter's length of the grid.

DIRECT NUMERICAL SIMULATION

The Computational Domain and Flow Conditions

Figure 2 shows the schematic of the computational domain. The computational domain size and number of grid points are listed in Table 2. The vertical (y) and spanwise (z) domain size is about 10 times of integral length scale. A turbulence-generating grid (classical grid or fractal square grid) is numerically constructed at $5.0M_{eff}$ from the

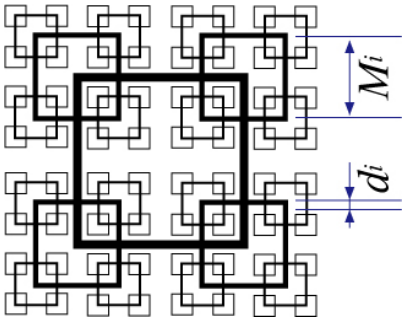

Figure 1: Schematic of the square type fractal grid.

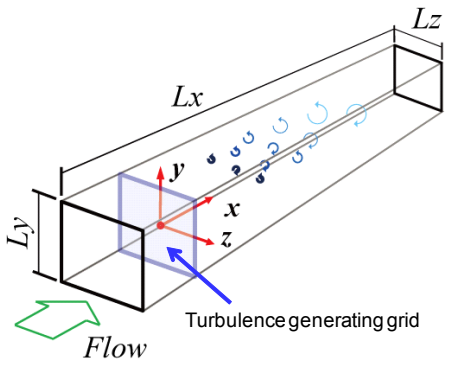

Figure 2: Schematic of computational domain.

entrance of the channel. The uniform flow is given as an inflow. The periodic boundary conditions for velocities are imposed in the vertical and spanwise directions. For Runs bCGT0 and sFGT0 (see Table 1), uniform scalar gradient is imposed in the vertical direction throughout the domain. The periodic boundary conditions for scalar are imposed in the vertical and spanwise directions. For Runs bCGT1 and sFGT1-3, a uniform passive scalar is supplied only from the upper stream, and therefore, the scalar mixing layers with an initial step profile develop downstream of the grids. For these cases, periodic boundary condition for the scalar is applied only to spanwise direction, and adiabatic condition is applied to vertical direction. For all cases, the convective outflow condition was applied at the exit, where the convection velocity was set at the same streamwise velocity averaged in y-z plane.

The Reynolds number based on the effective mesh size M_{eff} (Eq. 1), $\mathrm{Re}_M = U_o M_{eff}/\nu$, is set at 2,500 for all the cases, where U_o is the mean velocity and ν is the kinematic viscosity. It should be noted that the value of $\mathrm{Re}_M = 2,500$ for classical grid turbulence is not so small. In fact, the

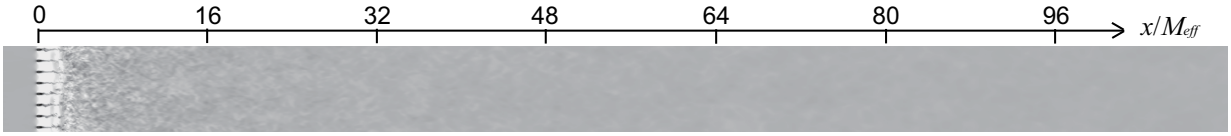

(a) by the classical grid (Run bCGT0)

(b) by the fractal square grid (Run sFGT0)

Figure 3: Instantaneous streamwise velocity fields at $z = 0$: white: $\tilde{u} = 1.5$; black: $\tilde{u} = -0.5$.

Table 2: The computational domain size and number of grid points

RunID	$Lx \times Ly \times Lz(M_{eff})$	$Nx \times Ny \times Nz$
bCGT0	$115.2 \times 8 \times 8$	$1280 \times 160 \times 160$
bCGT1	$64.0 \times 8 \times 8$	$1280 \times 160 \times 160$
sFGT0	$115.2 \times 16 \times 16$	$1280 \times 320 \times 320$
sFGT1	$64.0 \times 16 \times 16$	$768 \times 256 \times 256$
sFGT2	$64.0 \times 16 \times 16$	$768 \times 320 \times 320$
sFGT3	$64.0 \times 16 \times 16$	$768 \times 416 \times 416$

value is the same as those investigated in Nagata and Komori (2000, 2001), although round bars were used in these studies instead of rectangular bars simulated in this study. The DNS of classical grid turbulence at the same Re_M is also conducted for comparison (Runs bCGT0 and bCGT1). The Plandtl number Pr is 0.71 considering a turbulent diffusion of heat in an air flow.

The Governing Equations and Numerical Method

The governing equations are the continuity equation Eq. (2), forced incompressible Navier-Stokes equations Eq. (3), the transport equation for scalar Eq. (4) or scalar fluctuation Eq. (5)

$$\frac{\partial \tilde{u}_i}{\partial x_i} = 0, \tag{2}$$

$$\frac{\partial \tilde{u}_i}{\partial t} + \tilde{u}_j \frac{\partial \tilde{u}_i}{\partial x_j} = -\frac{\partial \tilde{p}}{\partial x_i} + \frac{1}{\mathrm{Re}_M} \frac{\partial^2 \tilde{u}_i}{\partial x_j \partial x_j} + F_i, \tag{3}$$

$$\frac{\partial \tilde{\theta}}{\partial t} + \tilde{u}_j \frac{\partial \tilde{\theta}}{\partial x_j} = \frac{1}{\mathrm{Re}_M \mathrm{Pr}} \frac{\partial^2 \tilde{\theta}}{\partial x_j \partial x_j}, \tag{4}$$

$$\frac{\partial \theta}{\partial t} + \tilde{u}_j \frac{\partial \theta}{\partial x_j} + \tilde{u_2} S_\Theta = \frac{1}{\mathrm{Re}_M \mathrm{Pr}} \frac{\partial^2 \theta}{\partial x_j \partial x_j}, \tag{5}$$

where $\tilde{u}_i$, $\tilde{p}$, $\tilde{\theta}$ and θ are instantaneous velocity, pressure, scalar and fluctuating scalar, respectively. In Eq.(3), the force term F_i is introduced to satisfy the nonslip boundary conditions on the grid surface by using the immersed boundary method (Fadlun et al., 2000). In Eq. (5), S_Θ is a uniform passive scalar gradient in the y ($i = 2$) direction for the case of bCGT0 and sFGT0.

To solve the govering equations, we constructed a numerical code based on fully conservative high order accurate finite difference schemes for full staggered grid systems (Morinishi et al., 1998), high order Runge-Kutta scheme for time advancement and Fast Fourier Transform (FFT) for the Poisson equation of pressure: the fractional step method based on the third-order Runge-Kutta method was used to solve the governing equations. The Poisson equation of pressure is solved by using the diagonal matrix algorithm in the streamwise direction and by the FFT in the vertical and spanwise directions. The staggered mesh arrangement is used to avoid spurious pressure oscillations. With the help of the concept of modified wavenumber, the divergence free condition is ensured up to the machine accuracy ($\sim O(10^{-14})$). Note that the Poisson equation was calculated in each Runge-Kutta step. The spatial resolution around the turbulence-generating grids is ensured by concentrating the grid points in the streamwise direction. Note that neither numerical filter nor numerical viscosity is used in the present DNS.

The convection terms in the vertical and spanwise directions are approximated by the fully conservative fourth-order central scheme and that in the streamwise direction by the fully conservative sixth-order central scheme for staggered grid systems. The viscous terms in the vertical and spanwise directions are calculated by the Fourier spectral method and that in the streamwise direction is approximated by the eighth-order cell centered mesh central compact scheme (Lele, 1992; Suzuki et al., 2009).

We have confirmed that our code has high accuracy by conducting a DNS of canonical channel flow with heat transfer and by comparing the results (fluctuating velocity, pressure, tempareture and budgets) with DNS database obtained by the spectral method (Iwamoto et al., 2002; Kasagi et al., 1992). The DNSs are conducted using a supercomputer NEC SX-8 of the Advanced Fluid Information, Research Center Institute of Fluid Science, Tohoku University.

RESULTS AND DISCUSSION

Flow Field

Instantaneous Field. Figure 3 show the instantaneous flow fields in the classical grid turbulence (Fig. 3a) and fractal grid turbulence (Fig. 3b). Here, the left side is the upstream. It is found that the turbulent scale in the fractal grid turbulence is larger than that in the classical grid turbulence. The turbulence intensities in the fractal grid turbulence are found to be much larger than those in the classical grid turbulence at the same mesh Reynolds num-

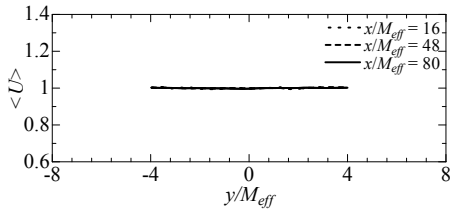

(a) by the classical grid

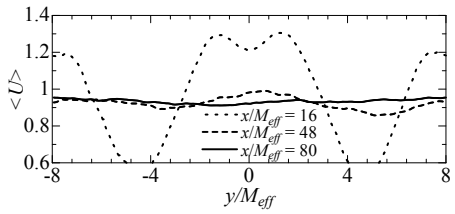

(b) by the fractal square grid

Figure 4: The vertical (y) profiles of mean velocity at $z = 0$.

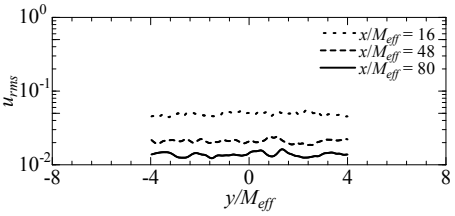

(a) by the classical grid

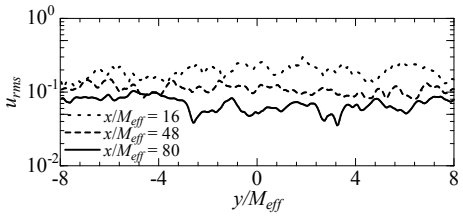

(b) by the fractal square grid

Figure 5: The vertical (y) profiles of fluctuating velocity at $z = 0$.

ber. The result agrees with the previous experiments (Hurst and Vassilicos, 2007; Seoud and Vassilicos, 2007).

Mean Velocity Profiles and Turbulence Intensities. Figure 4 shows the vertical profiles of mean velocity at $z = 0$. Figure 4(a) shows that the mean velocity profile is uniform in almost all region in the classical grid turbulence. Figure 4(b) shows that the mean velocity profile is almost uniform in the far downstream region of the fractal square grid.

Figure 5 shows the vertical profiles of fluctuating velocity at $z = 0$. Figure 5(a) shows that the turbulence intensities are approximately homogeneous across the vertical (and spanwise) direction in the downstream regions of the classical and fractal grids. It should be noted that the fractal grid generates high turbulence intensities compared with those generated by the classical grid at the same mesh Reynolds number.

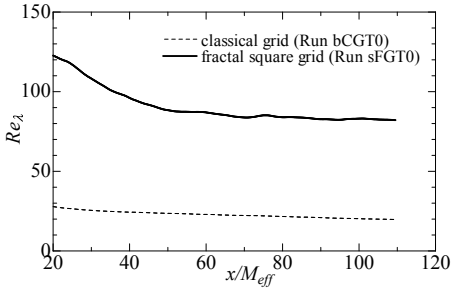

Figure 6: The streamwise profiles of turbulent Reynolds number based on the Taylor micro scale.

Turbulent Reynolds Number. Figure 6 shows the streamwise profiles of turbulent Reynolds number $Re_\lambda = u_{rms}\lambda/\nu$, where λ is the Taylor micro scale. In the classical grid turbulence, Re_λ slowly decays in the decaying region, and the value is $Re_\lambda \sim 20$ in the downstream region at $x/M_{eff} \sim 100$. In the fractal generated turbulence, on the other hand, the value of Re_λ is very large ($Re_\lambda \sim 80$ at $x/M_{eff} \sim 100$) despite the same mesh Reynolds number. Thus, as observed in Hurst and Vassilicos (2007) and Seoud and Vassilicos (2007), it is confirmed by the present DNS that the fractal grid generates high-Reynolds-number turbulence. For more information of the flow field, see our previous study (Nagata et al., 2008)

Temperature Field

Instantaneous Field. Figure 7 shows the instantaneous scalar fields in scalar mixing layers in the classical and fractal grid turbulence. The profiles in Fig. 7 suggest that typical scalar mixing layers are developed in the downstream region of the grids. It is confirmed that turbulent scalar mixing in the fractal grid turbulence (Figs. 7b∼d) is more enhanced compared with that in the classical grid turbulence (Fig. 7a).

Figure 8 shows the instantaneous fluctuating scalar fields in the classical and fractal grid turbulence. Since no scalar fluctuations exist at the inlet, the fluctuating scalar fields are generated by the grids. It can be seen that the scale and intensity of scalar fluctuations slowly increases in the downstream region. At the small scales, scalar fluctuation slowly decays in the downstream region by dissipation. This result qualitatively agrees with previous studies (Sirivat and Warhaft, 1983). In the fractal generated turbulence (Fig. 8b), large scalar fluctuations are generated compared with the classical grid turbulence (Fig. 8a).

Scalar Variances and Turbulent Scalar Flux (for Constant Mean Gradient). Figure 9 shows the streamwise profiles of turbulence intensities of scalar fluctuations for the constant mean gradient (Runs bCGT0 and sFGT0). In the classical grid turbulence (Run bCGT0), intensity of scalar fluctuations increases linearly (on the log-log plot) with increasing x/M_{eff}, which qualitatively agree with previous experiments (Sirivat and Warhaft, 1983). In the fractal grid turbulence (Run sFGT0), intensities of scalar fluctuations increases in the region $10 \leq x/M_{eff} \leq 30$, and the value is bigger than that in the classical grid turbulence. This result is consistent with the snapshot shown in Fig. 8. On the other hand, in the far downstream region of $x/M_{eff} > 30$,

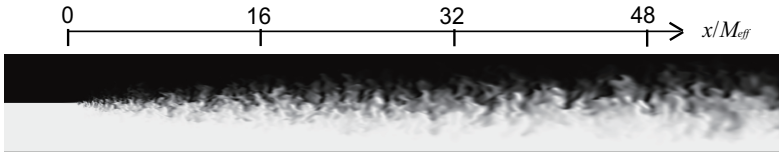

(a) by the classical grid (Run bCGT1)

(b) by the fractal square grid with $t_r = 5.0$ (Run bCGT2)

(c) by the fractal square grid with $t_r = 8.5$ (Run bCGT3)

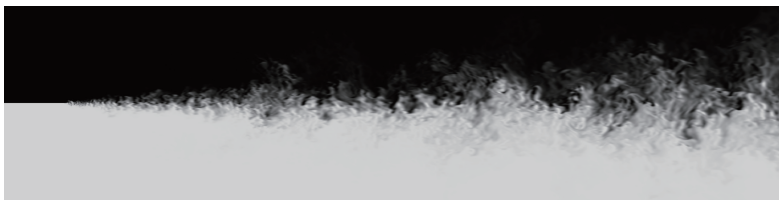

(d) by the fractal square grid with $t_r = 13.0$ (Run bCGT4)

Figure 7: Instantaneous scalar fields at $z = 0$ (scalar mixing layer).

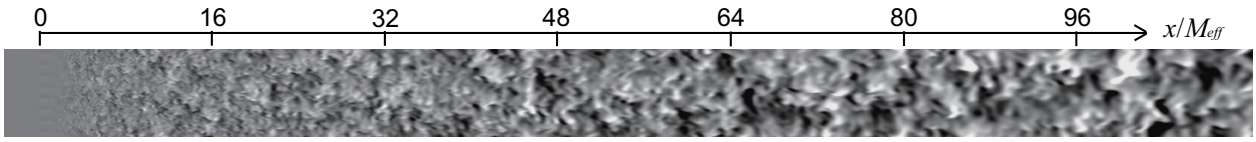

(a) by the classical grid (Run bCGT0)

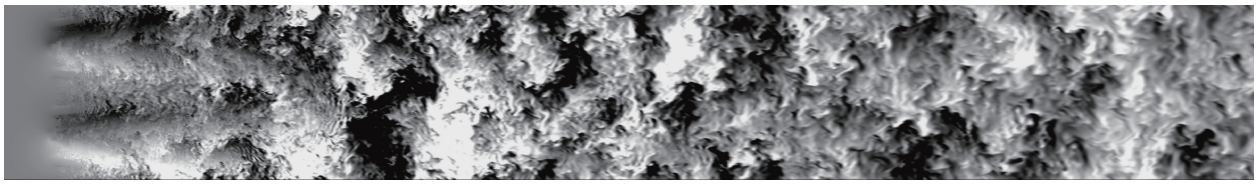

(b) by the fractal square grid (Run sFGT0)

Figure 8: Instantaneous fluctuating scalar fields at $z = 0$ (with a constant mean gradient).

intensity of scalar fluctuations decreases in the downstream direction.

Figure 10 shows the streamwise profiles of the vertical turbulent scalar flux (Runs bCGT0 and sFGT0). It is confirmed that turbulent scalar flux decreases slowly in the classical grid turbulence (Run bCGT0). In the fractal grid turbulence (Run sFGT0), it is confirmed that turbulent scalar flux is bigger than that in the classical grid turbulence.

CONCLUSIONS

The grid-generated turbulence using a classical biplane square grid and fractal grids with scalar transfer is investigated by means of the direct numerical simulation (DNS).

The fractal grid generates the high-Reynolds-number turbulence compared with the classical grid turbulence at the same mesh Reynolds number. For scalar mixing layer, turbulent scalar mixing in the fractal-grid turbulence is more

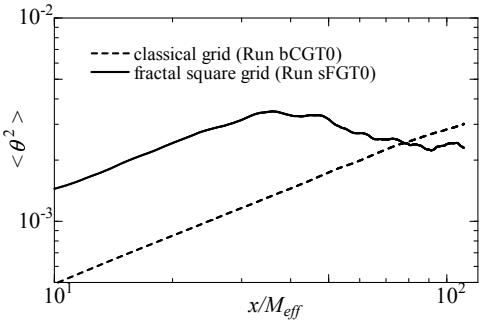

Figure 9: The streamwise profiles of turbulence intensities of scalar fluctuations.

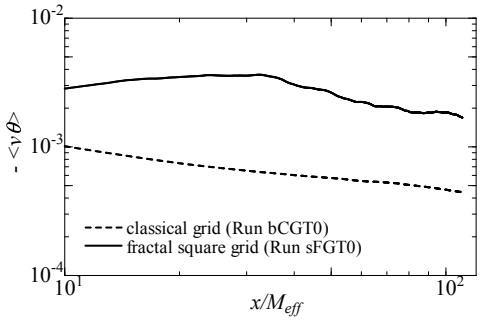

Figure 10: The streamwise profiles of the vertical turbulent scalar flux.

enhanced compared with that in the classical grid turbulence. For uniform scalar gradient, scalar fluctuation and turbulent scalar flux in the fractal grid turbulence is bigger than those in the classical grid turbulence.

ACKNOWLEDGEMENTS

The authors thank Professor J. Christos Vassilicos in Imperial College London for valuable comments to this study. The simulations are carried out using the supercomputer NEC SX-8 of the Advanced Fluid Information, Research Center Institute of Fluid Science, Tohoku University. The part of this study is supported by the Japanese Ministry of Education, Culture, Sports, Science and Technology through Grants-in-Aid (Nos. 18686015 and 20008010).

REFERENCES

Comte-Bellot, G., and Corrsin, S., 1966, "The Use of Contraction to Improve the Isotropy of Grid-Generated Turbulence", *Journal of Fluid Mechanics*, Vol. 24, pp. 657-682.

Fadlun, E. A., Verzicco, R., Orlandi, P., and Mohd-Yusof, J., 2000, "Combined Immersed-Boundary Finite-Difference Methods for Three-Dimensional Complex Flow Simulations", *Journal of Computational Physics*, Vol. 161, pp. 35-60.

Hurst, D., and Vassilicos, J. C., 2007, "Scalings and Decay of Fractal-Generated Turbulence", *Physics of Fluids*, Vol. 19, 035103.

Iwamoto, K., Suzuki, Y., and Kasagi, N., 2002, "Reynolds Number Effect on Wall Turbulence; Toward Effective Feedback Control", *Int. J. Heat and Fluid Flow*, Vol. 23 , pp. 678-689.

Kasagi, N., Tomita, Y., and Kuroda, A., 1992, "Direct Numerical Simulation of Passive Scalar Field in a Turbulent Channel Flow", *ASME J. Heat Transfer*, Vol. 114, pp. 598-606.

Laizet, S., and Vassilicos, J. C., 2008, "Multiscale Generation of Turbulence", *J. Multiscale Modelling*, in press.

Laizet, S., and Vassilicos, J. C., 2008, "A Numerical Strategy to Combine High-Order Schemes, Complex Geometry and Massively Parallel Computing for the DNS of Fractal Generated Turbulence", *Comput. and Fluids*, submitted.

Lele, S. K., 1992, "Compact Finite Difference Schemes with Spectral-Like Resolution", *Journal of Computational Physics*, Vol. 103, pp. 16-42.

Mazzi, B., and Vassilicos, J. C., 2004, "Fractal-Generated Turbulence", *Journal of Fluid Mechanics*, Vol. 502, pp. 65-87.

Morinishi, Y., Lund, T. S., Vasilyev, O. V., and Moin, P., 1998, "Fully Conservative Higher Order Finite Difference Schemes for Incompressible Flow", *Journal of Computational Physics*, Vol. 143, pp. 90-124.

Nagata, K., and Komori, S., 2000, "The Effects of Unstable Stratification and Mean Shear on the Chemical Reaction in Grid Turbulence", *J. Fluid Mech.*, Vol. 408, pp. 39-52.

Nagata, K., and Komori, S., 2001, "Difference in Turbulent Diffusion between Active and Passive Scalars in Stable Thermal- Stratification", *J. Fluid Mech.*, Vol. 430, pp. 361-380.

Nagata, K., Suzuki, H., Sakai, Y., Hayase, T., and Kubo, T., 2008, "Direct Numerical Simulation of Turbulence Characteristics Generated by Fractal Grids", *International Review of Physics*, Vol. 2, pp. 400-409.

Seoud, R. E., and Vassilicos, J. C., 2007, "Dissipation and Decay of Fractal-Generated Turbulence", *Physics of Fluids*, Vol. 19, 105108.

Sirivat, A., and Warhaft, Z., 1983, "The Effect of a Passive Cross-Stream Temperature Gradient on the Evolution of Temperature Variance and Heat Flux in Grid Turbulence", *Journal of Fluid Mechanics*, Vol. 128, pp. 323-346.

Suzuki, H., Nagata, K., Sakai, Y., Hayase, T., and Kubo, T., 2008, "DNS of Spatially Developing Fractal-Generated Turbulence", *Proc. of the 7th JSME-KSME Thermal and Fluids Engineering Conference*, in CD-ROM.

Suzuki, H., Nagata, K., Sakai, Y., Hayase, T., and Kubo, T., 2009, "Improvement of the DNS of Turbulent Channel Flow Using the Finite Difference Method (Introduction of the Compact Scheme to the Viscous Terms for High Spatial Resolution in the Dissipation Range) (in japanese)", *Transactions of the Japan Society of Mechanical Engineers, Series B*, in press.